ACSNANO
www.acsnano.org
ARTICLE

Big Effect of Small Nanoparticles: A Shift in Paradigm for Polymer Nanocomposites

Shiwang Cheng,[*,†] Shi-Jie Xie,[‡] Jan-Michael Y. Carrillo,[§,∥] Bobby Carroll,[⊥] Halie Martin,[#] Peng-Fei Cao,[†] Mark D. Dadmun,[†,#] Bobby G. Sumpter,[§,∥] Vladimir N. Novikov,[#] Kenneth S. Schweizer,[‡] and Alexei P. Sokolov[*,†,⊥,#]

[†]Chemical Sciences Division, [§]Computer Science and Mathematics Division, and [∥]Center for Nanophase Materials Sciences, Oak Ridge National Laboratory, Oak Ridge, Tennessee 37831, United States

[‡]Departments of Materials Science and Chemistry, Frederick Seitz Materials Research Laboratory, University of Illinois, Urbana, Illinois 61801, United States

[⊥]Department of Physics and Astronomy and [#]Department of Chemistry, University of Tennessee, Knoxville, Tennessee 37996, United States

Supporting Information

ABSTRACT: Polymer nanocomposites (PNCs) are important materials that are widely used in many current technologies and potentially have broader applications in the future due to their excellent property tunability, light weight, and low cost. However, expanding the limits in property enhancement remains a fundamental scientific challenge. Here, we demonstrate that well-dispersed, small (diameter ∼1.8 nm) nanoparticles with attractive interactions lead to unexpectedly large and qualitatively different changes in PNC structural dynamics in comparison to conventional nanocomposites based on particles of diameters ∼10−50 nm. At the same time, the zero-shear viscosity at high temperatures remains comparable to that of the neat polymer, thereby retaining good processability and resolving a major challenge in PNC applications. Our results suggest that the nanoparticle mobility and relatively short lifetimes of nanoparticle-polymer associations open qualitatively different horizons in the tunability of macroscopic properties in nanocomposites with a high potential for the development of advanced functional materials.

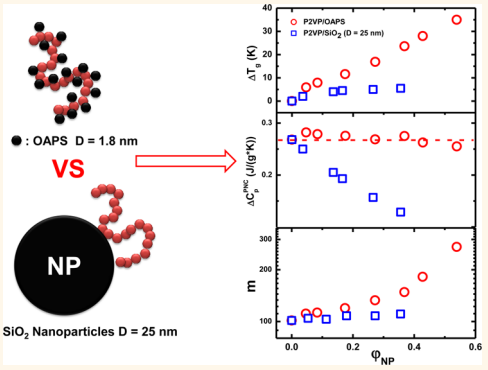

KEYWORDS: *polymer nanocomposites, small nanoparticles, glass transition, fragility, apparent disentanglement*

The addition of nanoparticles (NPs) to dense polymer matrices results in polymer nanocomposites (PNCs) with significantly altered segmental and chain relaxation,[1−3] leading to a wide tunability in macroscopic properties,[4−6] including the glass transition[1,2] and viscoelastic response.[3] An interfacial polymer layer of 1−5 nm thick surrounding NPs is well established[7−13] and has been regarded as the main mechanism of modifying macroscopic properties of PNCs.[14−18] Decreasing the NP size increases the interfacial layer volume fraction at fixed loading[15] and could enhance desirable changes. However, one expects that there is an optimum NP size since small enough particles typically plasticize the polymer matrix,[19−21] thereby speeding up dynamics, decreasing T_g, and reversing desirable thermomechanical property changes.[22] Moreover, weak interactions between polymer and NPs typically lead to aggregation and poor dispersion that often complicate studies of PNCs with small NPs, resulting in nonequilibrium effects and loss of interfacial area at high loadings.[22] As a result, only a few publications have analyzed the influence of small (diameter $D \sim$ 1−2 nm) well-dispersed NPs on PNC properties, although some revealed relatively large effects at low loadings (∼1−2 vol %).[23,24]

Here we present a detailed study of PNCs with well-dispersed, small (of the order of the polymer segment) attractive NPs. We discover unexpectedly large and qualitatively different dynamical effects relative to conventional PNCs with $D \sim$ 10−50 nm NPs. Combining experiment, theory, and simulations, we provide an understanding of these effects, which suggests a promising strategy for tuning macroscopic PNC properties over a considerably broader range than was previously possible.

Received: October 24, 2016
Accepted: January 4, 2017
Published: January 4, 2017

DOI: 10.1021/acsnano.6b07172
ACS Nano 2017, 11, 752−759

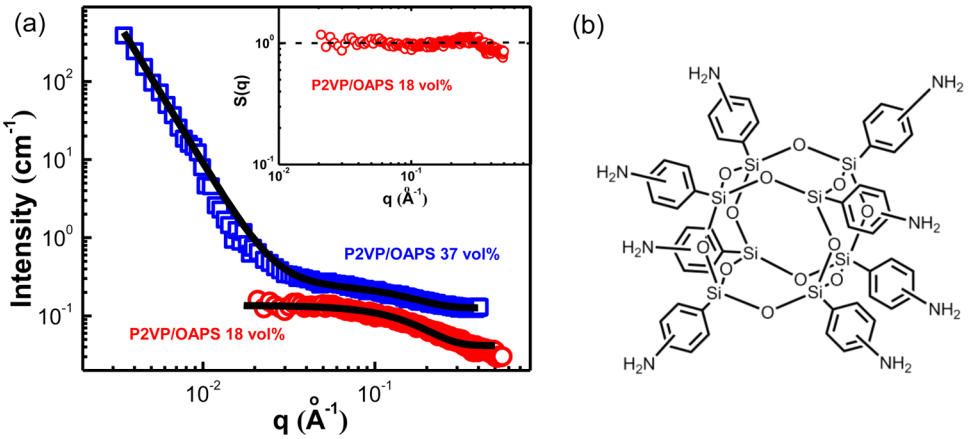

Figure 1. Reduced SAXS for P2VP/OAPS with φ_{OAPS} = 18 vol % and φ_{OAPS} = 37 vol %. The black lines show a fuzzy sphere model fit for φ_{OAPS} = 18 vol % and a combination of a power law and the fuzzy sphere model fit for φ_{OAPS} = 37 vol % (for details see the SI). The inset shows the corresponding static structure factor $S(q)$ (φ_{OAPS} = 18 vol %). (b) The chemical structure of OAPS, where the amine group can form hydrogen-bonds with both P2VP segments and OAPS particles.

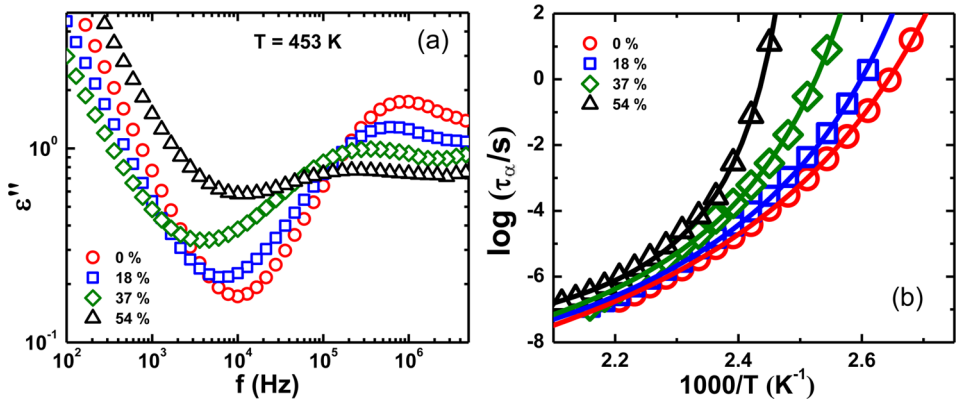

Figure 2. (a) Representative dielectric spectra of P2VP/OAPS with different loadings (in vol %) at 453 K, where the structural relaxation α-peak is well-defined. (b) Temperature dependence of τ_α for neat P2VP and P2VP/OAPS PNCs with different loadings.

RESULTS

We blend poly(2-vinylpyridine) (P2VP) (M_w = 101 kg/mol) with octaaminophenyl polyhedral oligomeric silsesquioxane (OAPS, Figure 1b) NPs of diameter D = 1.8 nm, nearly identical to the polymer Kuhn segment size, l_k ~ 1.7 nm. OAPS experiences strong hydrogen-bonding attractions with *both* itself and P2VP, with the latter allowing good dispersion. Details concerning sample preparation, characterization, and experimental protocol are presented in the Methods section and Supporting Information (SI).

Small-Angle X-ray Scattering (SAXS). SAXS has been used to analyze the OAPS dispersion in the nanocomposites. Detailed scattering data of all P2VP/OAPS are presented in Figure S1 in the SI. Figure 1a shows representative scattering intensity data $I(q)$ of OAPS in P2VP/OAPS (at φ_{OAPS} = 18 vol % and 37 vol %) obtained after subtracting the volume fraction weighted scattering of the pure P2VP melt. These results reveal excellent NP dispersion up to ~27 vol % that can be fit by a fuzzy sphere model (details of the fit procedure are presented in the SI). A representative static structure factor $S(q)$ of OAPS in P2VP (φ_{OAPS} = 18 vol %), converted from the scattering intensity $I(q)$ following the procedure proposed by Jouault *et al.*[25,26] (for details see the SI), shows a low q plateau value of ~1 (inset Figure 1a), which further supports dispersion at the single NP level. An increase of scattering intensity at low q (q < 0.02 Å^{-1}) for φ_{OAPS} = 37 vol % (Figure 1a) and higher is observed, indicating some spatial heterogeneity due to aggregation and/or kinetic gelation,[27] although the samples remain optically transparent up to φ_{OAPS} ~ 54 vol %.

Broadband Dielectric Spectroscopy (BDS). BDS was employed to probe segmental dynamics in these PNCs. The BDS data reveal large changes in the α-process peak with NP loading (Figure 2a): (i) a shift to lower frequency, (ii) broadening, and (iii) decreased amplitude. The segmental relaxation time is estimated from the peak frequency, $\tau_\alpha = 1/(2\pi f_p)$ and exhibits an unusually strong slowing down relative to the neat polymer at low temperatures (up to 6 decades at T ~ 410 K), which decreases to <1 decade at high temperatures (Figure 2b). The data also reveal a dramatic increase in T_g (defined by τ_α= 100 s) of up to ~35 K.

Temperature Modulated Differential Scanning Calorimetry (TMDSC). TMDSC measurements provide thermodynamic estimates of T_g. It is worth noting that there are no transition steps in DSC data of neat OAPS for T = 313−453 K (Figure S2 in the SI), signifying its high melting temperature or T_g. The PNC T_g, defined as the midpoint of the transition step, shifts from 372 to 407 K (Figure 3), consistent with the BDS measurements. This is an extraordinarily large increase compared to conventional PNCs with similar loading, *e.g.*, P2VP/SiO_2 (D = 25 nm) exhibits T_g shifts of only ~2−5 K

DOI: 10.1021/acsnano.6b07172
ACS Nano 2017, 11, 752−759

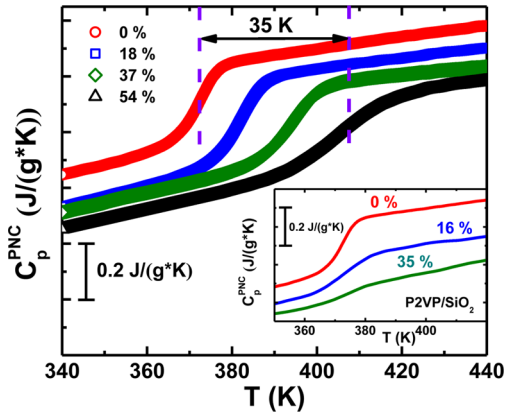

Figure 3. TMDSC measurement data of P2VP/OAPS nanocomposites with different loadings. Inset shows results for P2VP/SiO_2 with NP $D \sim 25$ nm (φ_{SiO_2} = 0 vol %, 16 vol %, and 35 vol %).

(Figures 3 and 5a).[8,10] The step amplitude, ΔC_p, of the P2VP/OAPS PNCs reveals another anomaly (Figure 5b): it remains almost constant ~0.27 J/(gK) despite a strong decrease in polymer weight fraction, which is again in qualitative contrast to conventional PNCs where ΔC_p scales well with polymer fraction (inset Figure 5b).[8,10]

Rheology. Rheology was employed to measure linear viscoelastic responses of both P2VP/OAPS and P2VP/SiO_2 PNCs. We used small amplitude oscillatory shear measurements, and the master curves of $G'(\omega)$ and $G''(\omega)$ spectra have been constructed using time−temperature superposition principles (Figure S3 in the SI). Figure 4a presents the $G'(\omega)$ and $G''(\omega)$ spectra of neat P2VP melt, P2VP/OAPS with φ_{OAPS} = 27 vol % and the conventional P2VP/SiO_2 with ϕ_{SiO_2} = 27 vol %, at T_{ref} = 453 K. The conventional P2VP/SiO_2 PNC shows the common gelation behavior, as indicated by a low-frequency power law $G' \sim G'' \sim \omega^{0.25}$, strong enhancement of the modulus, and absence of terminal flow[3] (Figure 4a). The rheological behavior of P2VP/OAPS at a similar loading is remarkably different and unexpected (Figure 4a): (i) the entanglement plateau modulus is almost identical to that of neat P2VP. (ii) Intermediate frequency (Rouse) dynamics are significantly slower, with an entanglement onset time, τ_e, ~11 times longer than in neat P2VP despite τ_α increasing only by a factor of ~1.9. (iii) The terminal flow time τ_d increases only by a factor of ~1.2. Consequently, the entanglement plateau breadth, quantified by τ_d/τ_e, shrinks from ~700 (neat P2VP) to ~70 at φ_{OAPS} = 27 vol % and to only ~5 at φ_{OAPS} = 37 vol % (Figure 4a and Figure S3 in the SI), indicating an apparent "disentanglement" in P2VP/OAPS. (iv) The complex viscosity, $|\eta^*|$, (inset Figure 4a) shows a zero-shear-rate plateau comparable to neat P2VP, in a sharp contrast to the ~1000 times increase for the conventional P2VP/SiO_2 PNC. Interestingly, the P2VP/OAPS nanocomposites do show gel-like behavior at loadings exceeding 43 vol % (Figures 4b and Figure S3 in the SI). Kinetic gelation in nanocomposites requiring such a high loading (especially for small NPs) is unexpected in the context of traditional PNCs.[28] However, a detailed discussion of the gelation behavior is beyond the scope of the current paper and will be considered in a future publication.

DISCUSSION

The presented experimental results reveal unexpectedly large and unusual effects of small sticky NPs on segmental dynamics, T_g, thermodynamic properties, and viscoelastic response of PNCs. There are seven key points.

(i) There is a dramatic increase in T_g of up to ~35 K, which is seen in *both* BDS and thermodynamic measurements (Figure 5a). This is in sharp contrast to a ~ 2−5 K increase in conventional P2VP/SiO_2 (D = 25 nm) PNCs[10] (Figure 5a) as well as another polymer/POSS nanocomposite that showed a reduction in T_g due to a plasticizer effect of small NPs.[30]

(ii) The temperature dependence of τ_α is usually quantified by the fragility index, $m = \left.\frac{d[\log_{10}\tau(T)]}{d(T_g/T)}\right|_{T=T_g}$. Remarkably, it grows enormously from m = 100 for neat P2VP to m = 270 for φ_{OAPS} = 54 vol % (Figure 5c), compared to a tiny ~10% change observed in conventional P2VP/SiO_2 PNCs (Figure 5c). Moreover, m = 270 is much higher than any value ever reported for polymer melts,[31] implying a sharp slowing down of dynamics with cooling

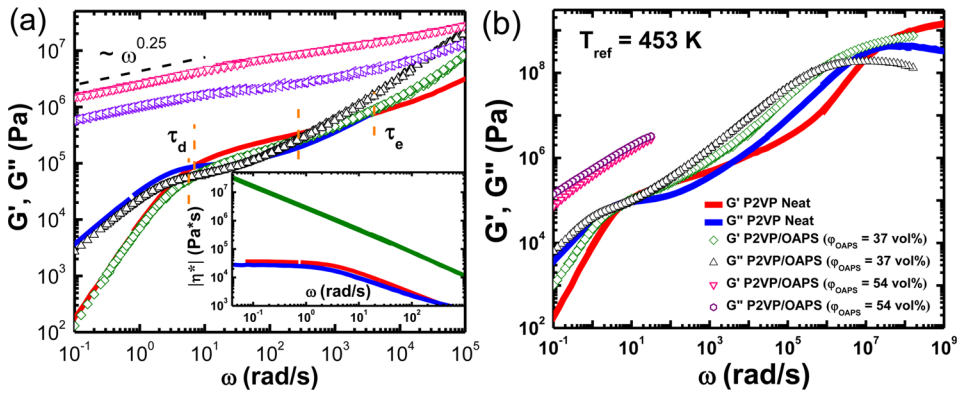

Figure 4. (a) Master curves constructed by time−temperature superposition of G' and G'' of P2VP/SiO_2 (φ_{SiO_2} = 27 vol %, pink and purple symbols), P2VP/OAPS (φ_{OAPS} = 27 vol %, olive, black symbols), and neat P2VP (red, blue lines) at T_{ref} = 453 K. Inset shows the complex viscosity, $|\eta^*|$, of neat P2VP (red), P2VP/OAPS (blue), and P2VP/SiO_2 (olive). (b) Master curves at T_{ref} = 453 K constructed using time−temperature superposition of G' and G'' for neat P2VP (red and blue lines), P2VP/OAPS (φ_{OAPS} = 37 vol %) (diamonds and upper triangles), and P2VP/OAPS (φ_{OAPS} = 54 vol %) (down triangles and hexagons).

DOI: 10.1021/acsnano.6b07172
ACS Nano 2017, 11, 752−759

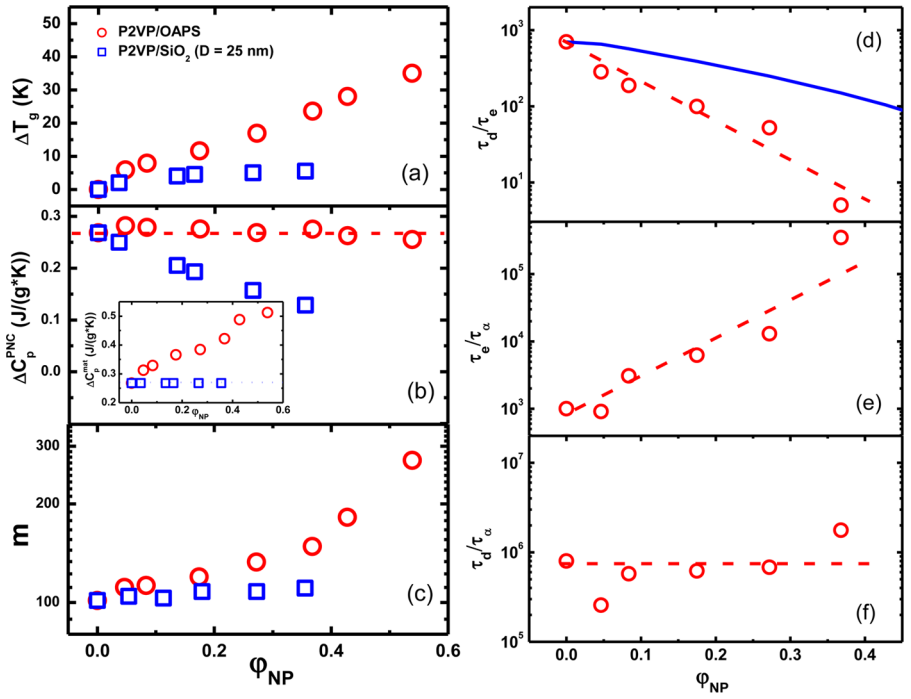

Figure 5. (a) Shift in the glass transition temperature, ΔT_g, (b) specific heat capacity jump at T_g, and (c) fragility index as a function of loading for P2VP/OAPS (red circles) and P2VP/SiO_2 (D_{SiO_2} = 25 nm) (blue squares). (d) Entanglement plateau length τ_d/τ_e, (e) entanglement onset to alpha time ratio, τ_e/τ_α, and (f) τ_d/τ_α ratio of P2VP/OAPS PNCs at different loadings. Inset in (b) shows that the ΔC_p of the matrix, $C_p^{mat} = \frac{C_p^{PNC} - C_p^{NP} m_{NP}}{1 - m_{NP}}$, appears to be independent of loading in the conventional PNCs, where C_p^{NP} and m_{NP} are the specific heat capacity and weight fraction of the NPs, respectively. The blue line in (d) is the dilution prediction of reptation tube theory.[29]

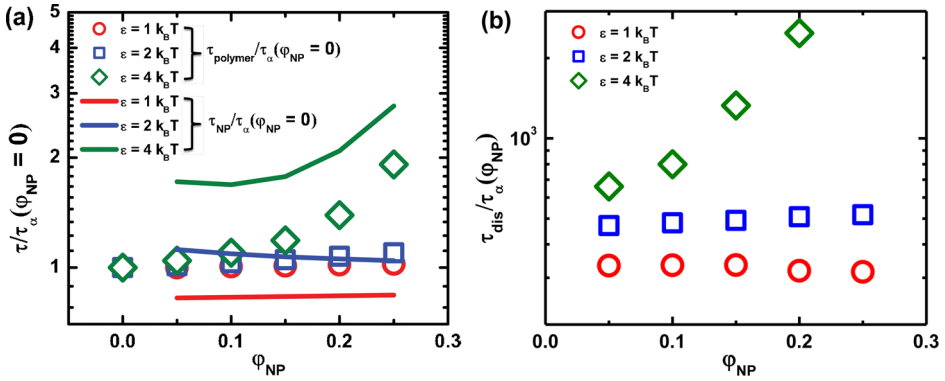

Figure 6. Simulation results for (a) the normalized alpha relaxation time of polymer segments ($\tau_{polymer}/\tau_\alpha(\varphi_{NP} = 0)$, symbols) and NPs ($\tau_{NP}/\tau_\alpha(\varphi_{NP} = 0)$, lines) and (b) normalized NP−segment dissociation time ($\tau_{dis}/\tau_\alpha(\varphi_{NP})$) as a function of loading at different polymer−NP interaction strength. At $\varepsilon = 1\ k_BT$, the interactions are purely repulsive, while the other ε's have attractions. See the SI for details.

and an unusual glass formation behavior of PNCs with small attractive NPs.

(iii) The specific heat capacity jump of the PNCs, ΔC_p^{PNC}, is almost independent of loading in P2VP/OAPS (Figure 3), while in P2VP/SiO_2 (D = 25 nm) PNCs, it monotonically decreases with loading. This strongly suggests that small NP mobility contributes in an essential manner to the kinetic vitrification and thermodynamics of OAPS-based PNCs.

(iv) The kinetic gelation that occurs in the conventional P2VP/SiO_2 (D = 25 nm) PNC is absent in P2VP/OAPS even at very high loading.

(v) Intriguingly, the breadth of the entanglement rubbery plateau, quantified by the time ratio τ_d/τ_e, decreases almost exponentially with loading (Figure 5d), $\tau_d/\tau_e \propto \exp(-13\varphi_{NP})$. This is much stronger than a power law dilution effect typically seen with addition of solvent or tiny NPs (blue line in Figure 5d).[29]

(vi) The ratio of the entanglement onset time to the structural relaxation (alpha) time, τ_e/τ_α, also increases exponentially with loading (Figure 5e), $\tau_e/\tau_\alpha \propto \exp(13\varphi_{NP})$. This violates the traditional idea that changes of segmental and chain modes with NP addition are fully coupled.

(vii) In contrast to points (v) and (vi), the ratio τ_d/τ_α is almost loading independent (Figure 5f), implying the dependence of the flow time and viscosity enhancements on loading is controlled entirely by the alpha relaxation.

DOI: 10.1021/acsnano.6b07172
ACS Nano 2017, 11, 752−759

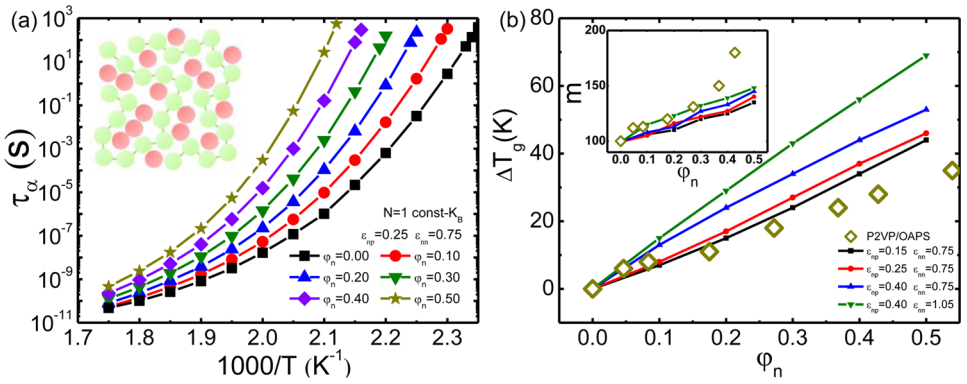

Figure 7. (a) Theoretical mean collective alpha time as a function of the inverse temperature for mixtures (ε_{pn} = 0.25, ε_{nn} = 0.75 in thermal energy units with T = 571 K) with various NP loading φ_n. Inset: Realistic sketch of the PNC with equally sized NP and Kuhn segment at φ_n = 33 vol %. (b) Glass transition temperature shift and fragility index (inset) predictions for various attraction strength parameters (lines), compared to experiment (symbols).

All these experimental results clearly demonstrate that P2VP/OAPS PNCs are in many respects qualitatively different from conventional PNCs[3,10−13,32] (Figure 5). Defining physical features of the latter, such as effectively immobile NPs, the formation of nanoscopic "bound adsorbed layers" on the surface of large NPs, and decoupling of dynamic and pseudo-thermodynamic measures of vitrification, are not applicable.[18]

To gain deeper insight, we performed coarse-grained (CG) molecular dynamics (MD) simulations (see Methods section and the SI for details) where the NP and polymer segment have an identical size and attract with an energy of 2−4 k_BT. The NP−NP and polymer−polymer interactions are repulsive, ensuring miscibility. The key findings are (Figure 6): (i) NPs and segments have comparable structural relaxation times, τ_{NP} = 1−2 τ_α, suggesting a very strong coupling of segment and NP motions, in qualitative contrast to conventional PNCs where NPs are essentially immobile on the segmental time scale. (ii) The time scale for relative NP-segment motion ("dissociation time"), τ_{dis}, estimated from the dynamic cross correlation function (see SI), is slower than the alpha process, increasing to $\tau_{dis} \sim 10^2$−10^3 τ_α for the strongest attraction. This suggests complete PNC structural relaxation involves two processes: cage relaxation and breaking of NP−polymer bonds, with the latter being slower.

Detailed comparisons of the simulations with experiment are inappropriate because the simulations are not in the deeply supercooled regime and NP−NP attraction is not included. To understand the deeply supercooled regime, we apply the recently developed "elastically collective nonlinear langevin equation" (ECNLE) approach, a quantitative theory of one-component molecular and polymer liquids.[33] Here it is extended to treat a binary mixture of equally sized NP and segment spheres to study their cooperative activated hopping, building on ideas successfully developed for colloidal mixtures[34] (see Methods section and the SI). For physical context, the inset of Figure 7a sketches the P2VP/OAPS PNC of interest and shows that at the relatively high loadings of primary interest, essentially every polymer segment is in contact with one or more NPs. Two attraction energy parameters (defined relative to the segment−segment attraction as a reference) between a segment and NP and between two NPs, ε_{pn} and ε_{nn}, respectively, are introduced. Their values are chosen based on chemical knowledge ($\varepsilon_{pn} < \varepsilon_{nn}$) and to ensure miscibility. Polymers are mapped to Kuhn length sized spheres and the mixture bulk modulus is kept constant. Details of the model, mapping and theory are presented in the Methods section and the SI.

Figure 7a shows theoretical calculations of the PNC mean alpha relaxation time for a specific choice of attraction energies at different loadings over a wide temperature range. By accounting for coupled activated motion of segments and NPs (which is predicted to occur on essentially the same mean time scale, see the SI), the theory qualitatively captures the basic experimental features (Figure 2b). Predictions for how the alpha time increases with NP loading at a fixed temperature are given in the SI. Figure 7b shows the T_g shift and fragility index results corresponding to Figure 7a for several different choices of attraction energies. They agree well with the large increases observed experimentally, including the distinctive nearly linear growth of T_g with loading. More broadly, the theoretical results illustrate how dynamic properties can be widely tuned by manipulating chemically specific attractions.

The physical picture that emerges from a detailed theoretical analysis (see SI) is that modestly sticky NPs form a limited number of physical bonds between themselves and with the polymer, resulting in extra dynamical constraints beyond steric caging, which increases the activation barrier, α-relaxation time, and T_g. The T_g shifts grow as either ε_{pn} or ε_{nn} increase. However, the correctly predicted roughly linear growth of T_g with loading does *not* occur if one unrealistically sets ε_{nn} = 0, and thus a NP−NP transient physical bond formation appears to be critical for the observed effects. The enhanced fragility has a structural and thermodynamic origin: As loading increases, more temperature-sensitive physical bonds form, and the growth of the PNC total packing fraction with cooling is enhanced. Importantly, a key idea suggested by theory and simulation that the alpha process involves cooperative motion of segments and NPs immediately provides a basis to understand the negligible change in the PNC heat capacity jump, ΔC_p, with loading (Figures 3 and 5b). The contribution of small NP motion to the specific heat compensates the loss of polymer weight fraction. We emphasize that the near equality of segment and NP relaxation time scales is a conseqeunce of *both* the relatively weak nature of the attractive interactions (and corresponding modest cohesive energy, see the SI) and the highly limited number of bonds a NP can form with the polymer given its small size. Either one or both of these features are absent in traditional PNC's which have well-defined, generally strongly bound layers of ∼ 1−5 nm thickness,[9−11]

DOI: 10.1021/acsnano.6b07172
ACS Nano 2017, 11, 752−759

typically resulting in a large time scale separation between NP motion and segmental relaxation.

Given the NP and segmental motions are strongly coupled, it seems unlikely that (all) physical bonds are broken by the alpha process, suggesting a longer time scale for complete structural rearrangement and initiation of chain-scale motions (*e.g.*, Rouse, reptation). Such a bond dissociation process can lead to a two-step structural relaxation (cage escape and bond breaking) in dense attractive colloid suspensions[35] and associating polymer liquids.[36,37] We expect that the dissociation time $\tau_{dis}(\varphi_{NP}) > \tau_\alpha(\varphi_{NP})$ and its ratio grow with loading, as suggested by simulation (Figure 6). Although the precise mechanism is unclear, we explore a simple physical idea, generically motivated by "sticky Rouse" models.[36,37] We postulate $\tau_{dis} \sim \tau_\alpha \exp(U_{NP}/k_BT)$, where the structural theory predicts the absolute value of the cohesive energy per particle $U_{NP} \propto \varphi_{NP}$ and $\tau_e(\varphi_{NP}) \propto \tau_{dis} \sim \tau_\alpha(\varphi_{NP}) \exp(b\varphi_{NP})$ with $b \sim 7-13$ (see the SI). The exponential enhancement of the entanglement onset time relative to the alpha time, and the magnitude of b, are consistent with experiment (Figure 5e). However, naively, this idea would seem to predict a stronger dependence of the flow time on loading than the alpha time, which is not observed (Figure 5f). One possibility is the slowing down of Rouse modes due to *small* sticky particles is a frictional effect which does not modify entanglement elastic properties. This speculation is consistent with our $\tau_e(\varphi_{NP})$ data (Figure 5e) and the loading independence of both $\tau_d(\varphi_{NP})/\tau_\alpha(\varphi_{NP})$ (Figure 5f) and the plateau modulus. More study is needed to draw definitive conclusions. But, the rheological behavior clearly does not follow standard "sticky Rouse"[36,37] or "sticky reptation"[38] models, where the terminal time grows due to a long "sticker lifetime". It also differs drastically from conventional PNCs (Figure 4), where nonequilibrium effects are caused by the exceptionally long chain-NP desorption times ($\sim 10^6-10^{12}\ \tau_\alpha$).[39]

CONCLUSIONS

Our studies reveal qualitatively different behaviors of PNC dynamics when NPs are sticky and comparable in size to a polymer segment. The tunable range of T_g and fragility far exceeds that previously found for conventional PNCs, while thermodynamic and viscoelastic properties show qualitatively unexpected small changes. We suggest all these results reflect the relatively fast mobility of small and moderately attractive NPs on the time scale of segmental dynamics which arises from the facile dissociation of the relatively weak and highly limited number of physical bonds between NPs and segments. The absence of significant viscosity change at high temperatures renders these PNCs very attractive in applications and processing. Our results suggest exciting opportunities for tuning macroscopic properties of PNCs over a range inaccessible with conventional PNCs by (i) controlling NP mobility *via* their size (in contrast to relatively immobile larger NPs) and (ii) by tuning the strength and lifetime of physical bonds *via* the rational chemical manipulation of attractive forces.

METHODS

Materials and Sample Preparations. Tetrahydrofuran (THF) was purchased from Sigma-Aldrich and used as received. Octaaminophenyl polyhedral oligomeric silsesquioxane (OAPS) was purchased from SES materials and used as received. Poly(2-vinylpyridine) (P2VP) with molecular weight (M_W) of 101 kg/mol and polydispersity of 1.07 was purchased from Scientific Polymer Source Inc. The OAPS powder was first dissolved in THF to prepare a stock solution of 0.15 g/mL. For polymer nanocomposites of each type, 0.3 g of polymers were first dissolved in 10 mL of THF to form polymer/THF solutions. Then, different amounts of OAPS/THF solution were added and mixed for 1 h. After that, the polymer/OAPS naocomposite solutions were poured into a Teflon dish to first dry under a hood for 24 h before being transferred to a vacuum oven (10^{-6} bar) under 160 °C for one more week. All the samples were characterized by thermogravimetric analysis (TGA) (TA Instruments Discover Q 50) under air with 20 °C/min heating up to 800 °C and temperature modulated differential scanning calorimetry (TMDSC) (TA Instruments, Q2000) with heating/cooling rate of 2 °C/min and modulation speed of ±0.5 °C/min. Mass densities of OAPS, SiO_2 NPs, and neat P2VP were 1.4028 ± 0.0019 g/cm^3, 2.4057 ± 0.0019 g/cm^3, and 1.2249 ± 0.0024 g/cm^3, respectively, and were measured by gas pycnometry (Micromeretics Accupyc II 1340).

Broadband Dielectric Spectroscopy Measurements. In the frequency range of $10^{-2}-10^7$ Hz, BDS measurements were carried out using a Novocontrol Concept-80 system with an Alpha-A impedance analyzer, a Quatro Cryosystem temperature controller, and a ZGS sample holder. PNC films of 0.08−0.15 mm were hot-pressed at 160 °C for P2VP/OAPS nanocomposites in a Teflon ring with inner diameter of 14 mm and outer diameter of 24 mm. These samples were then sandwiched by two gold-coated electrodes with a diameter of 20 mm before being transferred to the ZGS sample holder. All the measurements were conducted in the temperature range of 473−273 K with a step of 5 K between 473 K and 363 K and 10 K between 363 and 273 K. A thermal equilibration of 20 min was performed at each temperature before measurements.

Shear Rheology. Small amplitude oscillatory shear (SAOS) measurements were conducted on an AR2000ex rheometer (TA Instrument). For segmental relaxation and the glassy modulus, a parallel plate with a diameter of 4 mm and a strain amplitude of 0.05% was used. For rubbery plateau and terminal relaxation measurements, a parallel plate with a diameter of 8 mm and a strain amplitude of 1.0% was used. The temperature was controlled by an environmental test chamber under nitrogen atmosphere. The accuracy of the temperature was ±0.1 °C.

Small Angle X-ray Scattering. The SAXS measurements were performed at the Duke Shared Materials Instrumentation Facility using a high-flux SAXS instrument (SAXSLab Ganesha), a point collimated pinhole system with a 2D configurable detector and a Cu 50 kV Xenocs Genix ULD SL X-ray Source. All the measurements were performed at room temperature in transmission geometry on a series of thin nanocomposite films for a range of OAPS loadings. Scattering intensities measured as a function of half the scattering angle, θ, were first corrected for the absorption of the X-rays by the sample followed by further correction for the scattering of the empty cell and transformed to a plot of absolute scattering intensity *vs* momentum transfer vector, q ($q = 4\pi \sin \theta/\lambda$). The corrected data were normalized to absolute units with respect to the scattering of a water sample that is measured at exactly the same conditions as the P2VP/OAPS nanocomposite samples.

Molecular Dynamics Simulations. Coarse-grained (CG) molecular dynamics (MD) simulations based on the polymer melt model of Kremer and Grest,[40] but modified to include sticky NPs, were performed at the Oak Ridge Leadership Computing Facility (OLCF) using the LAMMPS[41,42] software package. The simulations contain 500 polymer chains with degree-of-polymerization of $N = 400$ which are mixed with varying amounts of sticky NPs of up to 25% by volume. Initially, the neat polymer melt was equilibrated using a combination of MD simulations and Monte Carlo bond swaps.[43] Thereafter, several copies of the equilibrated polymer melt were inserted with small NPs at random locations, resulting in several systems with different NP loadings. These were then equilibrated by slowly pushing off NPs that overlap with polymer segments in an equilibration MD run and followed by an equilibration MD run of $10^5\ \tau$ and a production MD run of $4 \times 10^5\ \tau$. The resulting particle trajectories were used to calculate the self-intermediate dynamic structure factor $F_s(t)$ and the

DOI: 10.1021/acsnano.6b07172
ACS Nano 2017, 11, 752−759

cross-correlation function between polymer segments and NPs $F_{12}(q,t)$. More details on the simulations and analysis of the simulation results are presented in the SI.

Theory. We considered two structural models of a P2VP/OAPS nanocomposite as a mixture of spherical hard NPs with polymers represented as either Kuhn length sized hard spheres or freely jointed chains (FJC) composed of N segments. Kuhn spheres or segments are equal in diameter to NPs to mimic the P2VP/OAPS system. When polymers are mapped to a liquid of either disconnected Kuhn-sized hard spheres or connected FJCs, their temperature-dependent (at 1 atm) dimensionless compressibilities are required to be identical to the experimentally known value.[33] As NPs are added, because the equation-of-state (EOS) of the P2VP/OAPS mixture is not experimentally available, we adopt two "calibration" strategies without introducing any adjustable parameters: keeping the mixture bulk modulus K_B or the pressure p constant. Details are in the SI.

NPs attract each other and the polymer segments *via* the pair potential:

$$U_{nj}(r) = -\varepsilon_{nj} e^{-(r-D)/\alpha D}, \quad r \geq \sigma_{nj}, \quad j = n, p \tag{1}$$

where α is a dimensionless spatial range parameter (set to 0.1 to mimic short-range hydrogen-bonding attractions). The choice of ε_{np} and ε_{nn} is described in the SI. The interaction between polymer segments is pure hard core $\varepsilon_{pp} = 0$. The structural pair correlation functions and static structure factors required to implement the dynamical theory are computed using standard Ornstein−Zernike integral equation theory[44] for the sphere mixture model and PRISM integral equation theory[45] when polymers are mapped to FJCs. The site−site Percus−Yevick closure approximation is adopted for all direct correlation functions.

The mixture nonlinear Langevin equation (NLE) theory[34] has been adopted to study the dynamics of P2VP/OAPS mixture. The key quantity is the so-called dynamic free energy surface as a function of displacement of the two species from their transiently localized positions ($\delta r_p = \delta r_n = 0$), $\delta r_n/\delta r_p$; it can be constructed from knowledge of the pair correlation structure of the mixture. The most important feature is the barrier height F_B along different paths defined by the ratio $\delta r_n/\delta r_p$. A representative calculation is shown in the SI. While it is now well-established that the NLE theory is a dynamic mean-field approach that captures only the local caging aspect of the activated relaxation process and significantly under predicts barriers in deeply supercooled liquid,[33,46] the "elastically collective nonlinear langevin equation" (ECNLE) theory for one component system has been developed[33,46] to include longer range collective effects based on the physical idea that elastic distortion of the surrounding liquid is required to allow a relatively large amplitude particle hopping on the cage scale.[33,46] We straightforwardly extend this idea to mixtures to calculate the required collective elastic barrier $F_{elastic}$ (see the SI). We find that, in accord with our physical intuition, the global minimum of the total barrier height $F_{total}(\equiv F_B + F_{elastic})$ is very close to $\delta r_n/\delta r_p = 1.0$ when polymers are mapped to either an effective hard sphere fluid or FJCs. Thus, the "most collective" trajectory path $\delta r_n/\delta r_p = 1.0$ is adopted to calculate the α relaxation time for all models under all conditions in this paper.

The mean barrier hopping time, which represents a collective hop of the two species following the maximally cooperative trajectory, follows as[33,46]

$$\tau_\alpha = \tau_s \left[1 + \frac{2\pi}{\sqrt{K_0 K_B}} e^{\beta(F_B + F_{elastic})} \right] \tag{2}$$

where K_0 and K_B are the absolute magnitudes of well and barrier positive curvature constants in units of k_BT/σ^2, respectively. The mean barrier hopping time is closely correlated with the structural alpha relaxation time.[47] For simplicity, τ_s is set to the realistic value of 10 ps, analogous to prior one-component liquid calculations.[46] We define T_g as when τ_α equals 100s. Dynamic fragility m is computed using the standard definition and our theoretically computed temperature-dependent alpha relaxation time.

ASSOCIATED CONTENT

Supporting Information

The Supporting Information is available free of charge on the ACS Publications website at DOI: 10.1021/acsnano.6b07172.

Detailed analysis of the small-angle X-ray scattering data; temperature modulated differential scanning calorimetry measurement of neat OAPS; master curves of loss and storage spectra from small amplitude oscillatory shear measurements; details of computer simulations and additional results; detailed descriptions of theory and additional results (PDF)

AUTHOR INFORMATION

Corresponding Authors

*E-mail: chengs@ornl.gov.
*E-mail: sokolov@utk.edu.

ORCID

Shiwang Cheng: 0000-0001-7396-4407
Shi-Jie Xie: 0000-0003-3317-4720
Jan-Michael Y. Carrillo: 0000-0001-8774-697X
Mark D. Dadmun: 0000-0003-4304-6087

Author Contributions

S.C., B.C., and A.S. carried out and designed the experiments. H.M. and M.D. performed and analyzed the SAXS measurements. S-J.X. and K.S. carried out the theoretical calculations. J-M.C. and B.S. performed the computer simulations.

Notes

The authors declare no competing financial interest.

ACKNOWLEDGMENTS

This work was supported by the U.S. Department of Energy, Office of Science, Basic Energy Sciences, Materials Science and Engineering Division. This research used resources of the Oak Ridge Leadership Computing Facility at Oak Ridge National Laboratory, which is supported by the Office of Science of the Department of Energy under Contract DE-AC05-00OR22725.

REFERENCES

(1) Bansal, A.; Yang, H. C.; Li, C. Z.; Cho, K. W.; Benicewicz, B. C.; Kumar, S. K.; Schadler, L. S. Quantitative Equivalence between Polymer Nanocomposites and Thin Polymer Films. *Nat. Mater.* **2005**, *4*, 693−698.

(2) Rittigstein, P.; Priestley, R. D.; Broadbelt, L. J.; Torkelson, J. M. Model Polymer Nanocomposites Provide an Understanding of Confinement Effects in Real Nanocomposites. *Nat. Mater.* **2007**, *6*, 278−282.

(3) Baeza, G. P.; Dessi, C.; Costanzo, S.; Zhao, D.; Gong, S.; Alegria, A.; Colby, R. H.; Rubinstein, M.; Vlassopoulos, D.; Kumar, S. K. Network Dynamics in Nanofilled Polymers. *Nat. Commun.* **2016**, *7*, 11368.

(4) Balazs, A. C.; Emrick, T.; Russell, T. P. Nanoparticle Polymer Composites: Where Two Small Worlds Meet. *Science* **2006**, *314*, 1107−1110.

(5) Hussain, F.; Hojjati, M.; Okamoto, M.; Gorga, R. E. Review Article: Polymer-Matrix Nanocomposites, Processing, Manufacturing, and Application: An Overview. *J. Compos. Mater.* **2006**, *40*, 1511−1575.

(6) Jancar, J.; Douglas, J. F.; Starr, F. W.; Kumar, S. K.; Cassagnau, P.; Lesser, A. J.; Sternstein, S. S.; Buehler, M. J. Current Issues in Research on Structure-Property Relationships in Polymer Nanocomposites. *Polymer* **2010**, *51*, 3321−3343.

(7) Papon, A.; Montes, H.; Hanafi, M.; Lequeux, F.; Guy, L.; Saalwächter, K. Glass-Transition Temperature Gradient in Nano-

DOI: 10.1021/acsnano.6b07172
ACS Nano 2017, 11, 752−759

composites: Evidence from Nuclear Magnetic Resonance and Differential Scanning Calorimetry. *Phys. Rev. Lett.* **2012**, *108*, 065702.
(8) Moll, J.; Kumar, S. K. Glass Transitions in Highly Attractive Highly Filled Polymer Nanocomposites. *Macromolecules* **2012**, *45*, 1131−1135.
(9) Jouault, N.; Moll, J. F.; Meng, D.; Windsor, K.; Ramcharan, S.; Kearney, C.; Kumar, S. K. Bound Polymer Layer in Nanocomposites. *ACS Macro Lett.* **2013**, *2*, 371−374.
(10) Holt, A. P.; Griffin, P. J.; Bocharova, V.; Agapov, A. L.; Imel, A. E.; Dadmun, M. D.; Sangoro, J. R.; Sokolov, A. P. Dynamics at the Polymer/Nanoparticle Interface in Poly(2-Vinylpyridine)/Silica Nanocomposites. *Macromolecules* **2014**, *47*, 1837−1843.
(11) Gong, S.; Chen, Q.; Moll, J. F.; Kumar, S. K.; Colby, R. H. Segmental Dynamics of Polymer Melts with Spherical Nanoparticles. *ACS Macro Lett.* **2014**, *3*, 773−777.
(12) Cheng, S.; Holt, A. P.; Wang, H.; Fan, F.; Bocharova, V.; Martin, H.; Etampawala, T.; White, B. T.; Saito, T.; Kang, N.-G.; et al. Unexpected Molecular Weight Effect in Polymer Nanocomposites. *Phys. Rev. Lett.* **2016**, *116*, 038302.
(13) Holt, A. P.; Bocharova, V.; Cheng, S.; Kisliuk, A. M.; White, B. T.; Saito, T.; Uhrig, D.; Mahalik, J. P.; Kumar, R.; Imel, A. E.; et al. Controlling Interfacial Dynamics: Covalent Bonding Versus Physical Adsorption in Polymer Nanocomposites. *ACS Nano* **2016**, *10*, 6843−6852.
(14) Berriot, J.; Montes, H.; Lequeux, F.; Long, D.; Sotta, P. Evidence for the Shift of the Glass Transition near the Particles in Silica-Filled Elastomers. *Macromolecules* **2002**, *35*, 9756−9762.
(15) Schadler, L. S.; Kumar, S. K.; Benicewicz, B. C.; Lewis, S. L.; Harton, S. E. Designed Interfaces in Polymer Nanocomposites: A Fundamental Viewpoint. *MRS Bull.* **2007**, *32*, 335−340.
(16) Papon, A.; Montes, H.; Lequeux, F.; Oberdisse, J.; Saalwachter, K.; Guy, L. Solid Particles in an Elastomer Matrix: Impact of Colloid Dispersion and Polymer Mobility Modification on the Mechanical Properties. *Soft Matter* **2012**, *8*, 4090−4096.
(17) Cheng, S.; Bocharova, V.; Belianinov, A.; Xiong, S.; Kisliuk, A.; Somnath, S.; Holt, A. P.; Ovchinnikova, O. S.; Jesse, S.; Martin, H.; et al. Unraveling the Mechanism of Nanoscale Mechanical Reinforcement in Glassy Polymer Nanocomposites. *Nano Lett.* **2016**, *16*, 3630−3637.
(18) Starr, F. W.; Douglas, J. F.; Meng, D.; Kumar, S. K. Bound Layers "Cloak" Nanoparticles in Strongly Interacting Polymer Nanocomposites. *ACS Nano* **2016**, *10*, 10960.
(19) Tuteja, A.; Mackay, M. E.; Narayanan, S.; Asokan, S.; Wong, M. S. Breakdown of the Continuum Stokes−Einstein Relation for Nanoparticle Diffusion. *Nano Lett.* **2007**, *7*, 1276−1281.
(20) Cai, L.-H.; Panyukov, S.; Rubinstein, M. Mobility of Nonsticky Nanoparticles in Polymer Liquids. *Macromolecules* **2011**, *44*, 7853−7863.
(21) Yamamoto, U.; Schweizer, K. S. Microscopic Theory of the Long-Time Diffusivity and Intermediate-Time Anomalous Transport of a Nanoparticle in Polymer Melts. *Macromolecules* **2015**, *48*, 152−163.
(22) Nusser, K.; Schneider, G. J.; Pyckhout-Hintzen, W.; Richter, D. Viscosity Decrease and Reinforcement in Polymer−Silsesquioxane Composites. *Macromolecules* **2011**, *44*, 7820−7830.
(23) Kropka, J. M.; Sakai, V. G.; Green, P. F. Local Polymer Dynamics in Polymer-C-60 Mixtures. *Nano Lett.* **2008**, *8*, 1061−1065.
(24) Kuo, S.-W.; Chang, F.-C. Poss Related Polymer Nanocomposites. *Prog. Polym. Sci.* **2011**, *36*, 1649−1696.
(25) Jouault, N.; Dalmas, F.; Said, S.; Di Cola, E.; Schweins, R.; Jestin, J.; Boué, F. Direct Small-Angle-Neutron-Scattering Observation of Stretched Chain Conformation in Nanocomposites: More Insight on Polymer Contributions in Mechanical Reinforcement. *Phys. Rev. E* **2010**, *82*, 031801.
(26) Jouault, N.; Dalmas, F.; Said, S.; Di Cola, E.; Schweins, R.; Jestin, J.; Boué, F. Direct Measurement of Polymer Chain Conformation in Well-Controlled Model Nanocomposites by Combining Sans and Saxs. *Macromolecules* **2010**, *43*, 9881−9891.
(27) Akcora, P.; Liu, H.; Kumar, S. K.; Moll, J.; Li, Y.; Benicewicz, B. C.; Schadler, L. S.; Acehan, D.; Panagiotopoulos, A. Z.; Pryamitsyn, V.; et al. Anisotropic Self-Assembly of Spherical Polymer-Grafted Nanoparticles. *Nat. Mater.* **2009**, *8*, 354−U121.
(28) Chen, Q.; Gong, S.; Moll, J.; Zhao, D.; Kumar, S. K.; Colby, R. H. Mechanical Reinforcement of Polymer Nanocomposites from Percolation of a Nanoparticle Network. *ACS Macro Lett.* **2015**, *4*, 398−402.
(29) Doi, M.; Edwards, S.F. *The Theory of Polymer Dynamics*; Oxford University Press: New York, 1986.
(30) Kopesky, E. T.; Haddad, T. S.; Cohen, R. E.; McKinley, G. H. Thermomechanical Properties of Poly(Methyl Methacrylate)S Containing Tethered and Untethered Polyhedral Oligomeric Silsesquioxanes. *Macromolecules* **2004**, *37*, 8992−9004.
(31) Sokolov, A. P.; Novikov, V. N.; Ding, Y. Why Many Polymers Are So Fragile. *J. Phys.: Condens. Matter* **2007**, *19*, 205116.
(32) Cheng, S.; Mirigian, S.; Carrillo, J.-M. Y.; Bocharova, V.; Sumpter, B. G.; Schweizer, K. S.; Sokolov, A. P. Revealing Spatially Heterogeneous Relaxation in a Model Nanocomposite. *J. Chem. Phys.* **2015**, *143*, 194704.
(33) Mirigian, S.; Schweizer, K. S. Dynamical Theory of Segmental Relaxation and Emergent Elasticity in Supercooled Polymer Melts. *Macromolecules* **2015**, *48*, 1901−1913.
(34) Viehman, D. C.; Schweizer, K. S. Cooperative Activated Dynamics in Dense Mixtures of Hard and Sticky Spheres. *Phys. Rev. E* **2008**, *78*, 051404.
(35) Pham, K. N.; Puertas, A. M.; Bergenholtz, J.; Egelhaaf, S. U.; Moussaïd, A.; Pusey, P. N.; Schofield, A. B.; Cates, M. E.; Fuchs, M.; Poon, W. C. K. Multiple Glassy States in a Simple Model System. *Science* **2002**, *296*, 104−106.
(36) Rubinstein, M.; Semenov, A. N. Dynamics of Entangled Solutions of Associating Polymers. *Macromolecules* **2001**, *34*, 1058−1068.
(37) Chen, Q.; Tudryn, G. J.; Colby, R. H. Ionomer Dynamics and the Sticky Rouse Model. *J. Rheol.* **2013**, *57*, 1441−1462.
(38) Leibler, L.; Rubinstein, M.; Colby, R. H. Dynamics of Reversible Networks. *Macromolecules* **1991**, *24*, 4701−4707.
(39) Napolitano, S.; Wubbenhorst, M. The Lifetime of the Deviations from Bulk Behaviour in Polymers Confined at the Nanoscale. *Nat. Commun.* **2011**, *2*, 260.
(40) Kremer, K.; Grest, G. S. Dynamics of Entangled Linear Polymer Melts: A Molecular-Dynamics Simulation. *J. Chem. Phys.* **1990**, *92*, 5057−5086.
(41) Plimpton, S. Fast Parallel Algorithms for Short-Range Molecular Dynamics. *J. Comput. Phys.* **1995**, *117*, 1−19.
(42) Brown, W. M.; Wang, P.; Plimpton, S. J.; Tharrington, A. N. Implementing Molecular Dynamics on Hybrid High Performance Computers−Short Range Forces. *Comput. Phys. Commun.* **2011**, *182*, 898−911.
(43) Auhl, R.; Everaers, R.; Grest, G. S.; Kremer, K.; Plimpton, S. J. Equilibration of Long Chain Polymer Melts in Computer Simulations. *J. Chem. Phys.* **2003**, *119*, 12718−12728.
(44) Hansen, J. P.; McDonald, I. R. *Theory of Simple Liquids*; Academic Press Limited: London, 1986.
(45) Hall, L. M.; Schweizer, K. S. Many Body Effects on the Phase Separation and Structure of Dense Polymer-Particle Melts. *J. Chem. Phys.* **2008**, *128*, 234901.
(46) Mirigian, S.; Schweizer, K. S. Elastically Cooperative Activated Barrier Hopping Theory of Relaxation in Viscous Fluids. Ii. Thermal Liquids. *J. Chem. Phys.* **2014**, *140*, 194507.
(47) Schweizer, K. S.; Saltzman, E. J. Entropic Barriers, Activated Hopping, and the Glass Transition in Colloidal Suspensions. *J. Chem. Phys.* **2003**, *119*, 1181−1196.

DOI: 10.1021/acsnano.6b07172
ACS Nano 2017, 11, 752−759